

S1: Full details of U-Pb analysis

Samples were screened and analysed in situ from polished sections using a RESOLution 193 nm ArF excimer laser (CompexPro 102) equipped with a two-volume ablation cell (Laurin Technic S155) coupled to a sector field ICP-MS (ElementXr, ThermoScientific) at FIERCE (Frankfurt Isotope & Element Research Center), Goethe-University Frankfurt. Ablation was performed in a He atmosphere (0.3 l/min) and mixed in the ablation funnel with 1.1 l/min Ar and 0.06 l/min N. Signal strength at the ICP-MS was tuned for maximum sensitivity while keeping oxide formation below 0.2 % (UO/U) and element fraction low (e.g., Th/U ~ 1). Static ablation used a spot size of 188 µm (squared shape) and a fluence of c. 2 J/cm² at 12 Hz. This yielded for SRM-NIST 614 a depth penetration of c. 0.6 µm/s and an average sensitivity of 1.1×10^6 cps/ppm for ²³⁸U. Data were acquired in fully-automated mode overnight. Each analysis consists of 18 s of background acquisition followed by 18 s of sample ablation and 23 s washout. During 36 s data acquisition, the signal of ²⁰⁶Pb, ²⁰⁷Pb, ²³²Th, and ²³⁸U were detected by peak jumping in pulse counting mode with a total integration time of 0.99 s, resulting in 370 mass scans.

Raw data were corrected offline using an in-house Microsoft Excel spreadsheet program (Gerdes and Zeh, 2006, 2009). Following background correction, outliers ($\pm 2\sigma$) were rejected based on the time-resolved ²⁰⁷Pb/²⁰⁶Pb and ²⁰⁶Pb/²³⁸U ratios and the Pb and U signal. Due to fast washout, the low volume cell allows detecting inhomogeneity of the ablated material during depth profiling at a level of <0.8 mm (<1 s).

Before the analysis, the samples were checked, whether they are suitable for U-Pb dating. For this purpose, the laser was manually moved over the section guided by transmitted light and cathode-luminescence images, fired for 3–5 s per spot, and at the same time, the Pb and U signal and their isotope ratios monitored on the screen. Typically, 10–30 points for each carbonate phase are identified in areas with variable ²³⁸U/²⁰⁶Pb and ²⁰⁷Pb/²⁰⁶Pb within 10–15 min. This procedure allows within one day to screen 20–40 different carbonate domains (e.g., veins, cement...) from up to 16 polished sections and subsequently analyse them in an automatized sequence overnight.

Soda-lime glass SRM-NIST 614 (n = 28) was used as a primary reference to correct for mass bias (²⁰⁷Pb/²⁰⁶Pb, c. 0.2 %) and inter-element fractionation (²⁰⁶Pb/²³⁸U, c. 30 %) and their drift through the entire analytical sequence (c. 12 h). SRM-NIST 614 was analysed in duplicate together with two carbonate reference material every 35–40 min.

For carbonates, an additional matrix correction of 10 % has been applied on the ²⁰⁶Pb/²³⁸U based on analyses of WC-1 carbonate reference material (254.0 ± 6.4 Ma; Roberts et al., 2017). During sequence 1 and 2 the WC-1 (n = 28) yielded an ²⁰⁶Pb/²³⁸U lower intercept age of 253.7 ± 2.1 Ma (2σ, MSWD = 1.6) and 253.9 ± 1.3 Ma (2σ, MSWD = 1.15), respectively.

ASH15-D analysed as secondary reference material (n = 28) gave a lower intercept age of 2.98 ± 0.10 Ma (2σ, MSWD = 1.07, sequence 1) and 2.966 ± 0.088 Ma (2σ, MSWD = 1.02, sequence 2). This is identical within the uncertainty of the U-Pb age from two labs (3.085 ± 0.044 and 3.005 ± 0.026 Ma; Vaks et al., 2003) using the conventional U-Pb method (ID TIMS).

Data points of each carbonate phase derived from a small area (<1 cm²) and defining linear arrays in the ²⁰⁷Pb/²⁰⁶Pb vs. ²³⁸U/²⁰⁶Pb space (Tera-Wasserburg diagram) interpreted to be a mixture of initial common-Pb and Pb that formed due to in situ decay of U since mineralization. The age of formation is defined by the lower intercept with the Concordia. Plots and ages were calculated using Isoplot 3.71 (Ludwig, 2007). All uncertainties are reported at the 2σ level.

An excel file with a LA-ICP-MS U-Th-Pb data report and tables with data of all samples and reference material is provided with this appendix.

References:

- Gerdes A. and Zeh A. (2006) Combined U-Pb and Hf isotope LA- (MC-) ICP-MS analyses of detrital zircons: comparison with SHRIMP and new constraints for the provenance and age of an Armorican metasediment in Central Germany. *Earth Planet. Sci. Lett.* 249, 47–61.
- Gerdes A. and Zeh A. (2009) Zircon formation versus zircon alteration—new insights from combined U-Pb and Lu-Hf in situ LA-ICP-MS analyses, and consequences for the interpretation of Archean zircon from the Central Zone of the Limpopo Belt. *Chem. Geol.* 261, 230–243.
- Ludwig K. (2007) Isoplot 3.62. Berkeley Geochronology Center Special Publication, 470.
- Roberts N. M., Rasbury E. T., Parrish R. R., Smith C. J., Horstwood M. S. and Condon D. J. (2017) A calcite reference material for LA-ICP-MS U-Pb geochronology. *Geochem. Geophys. Geosyst.* 18, 2807–2814.
- Vaks A., Bar-Matthews M., Ayalona A., Schilman B., Gilmour B., Hawkesworth C. J., Frumkin A., Kaufman A. and Matthews A. (2003) Paleoclimate reconstruction based on the timing of speleothem growth and oxygen and carbon isotope composition in a cave located in the rain shadow in Israel. *Quat. Res.* 59, 182–193.

Sequence 1
(continues on next page)

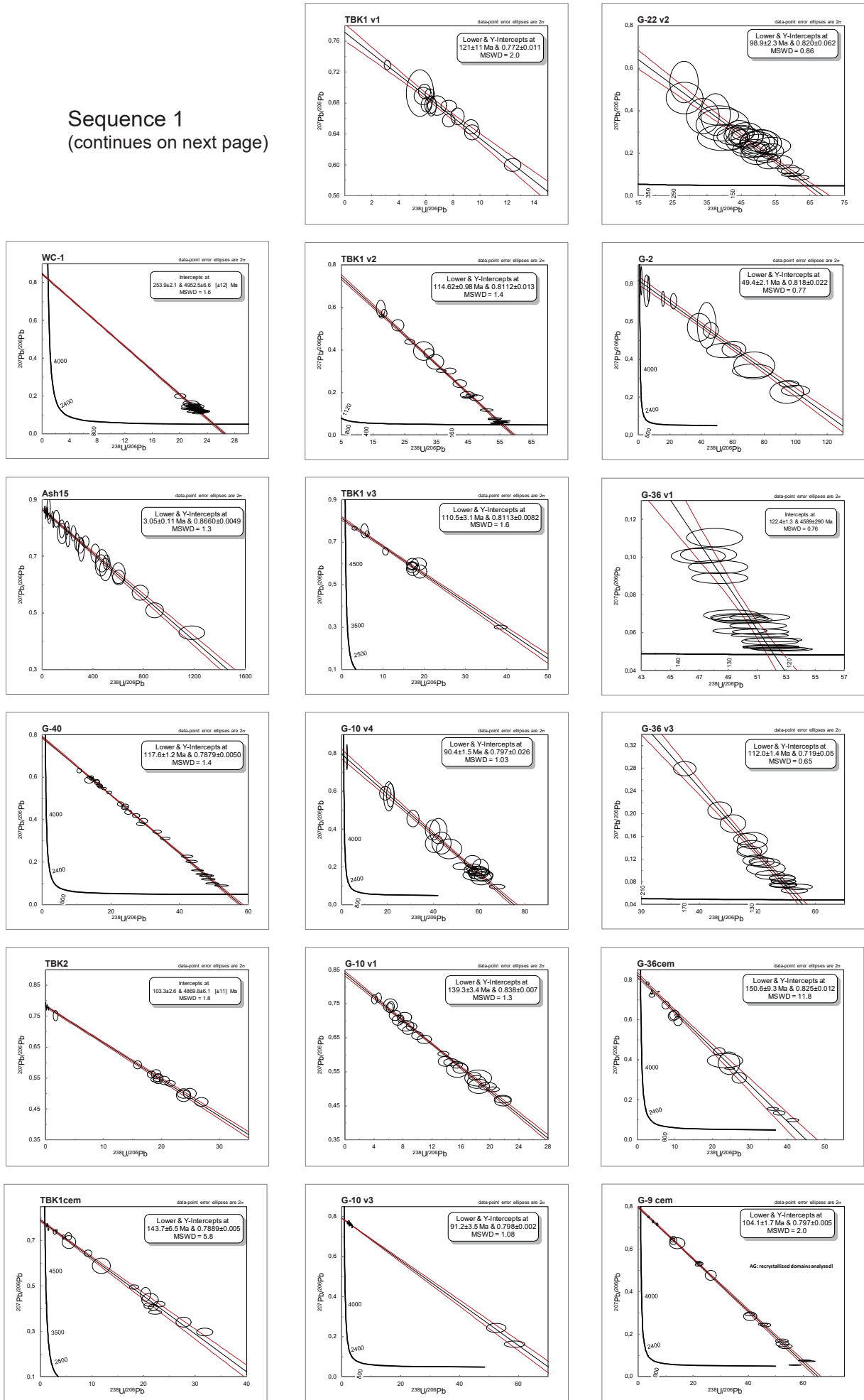
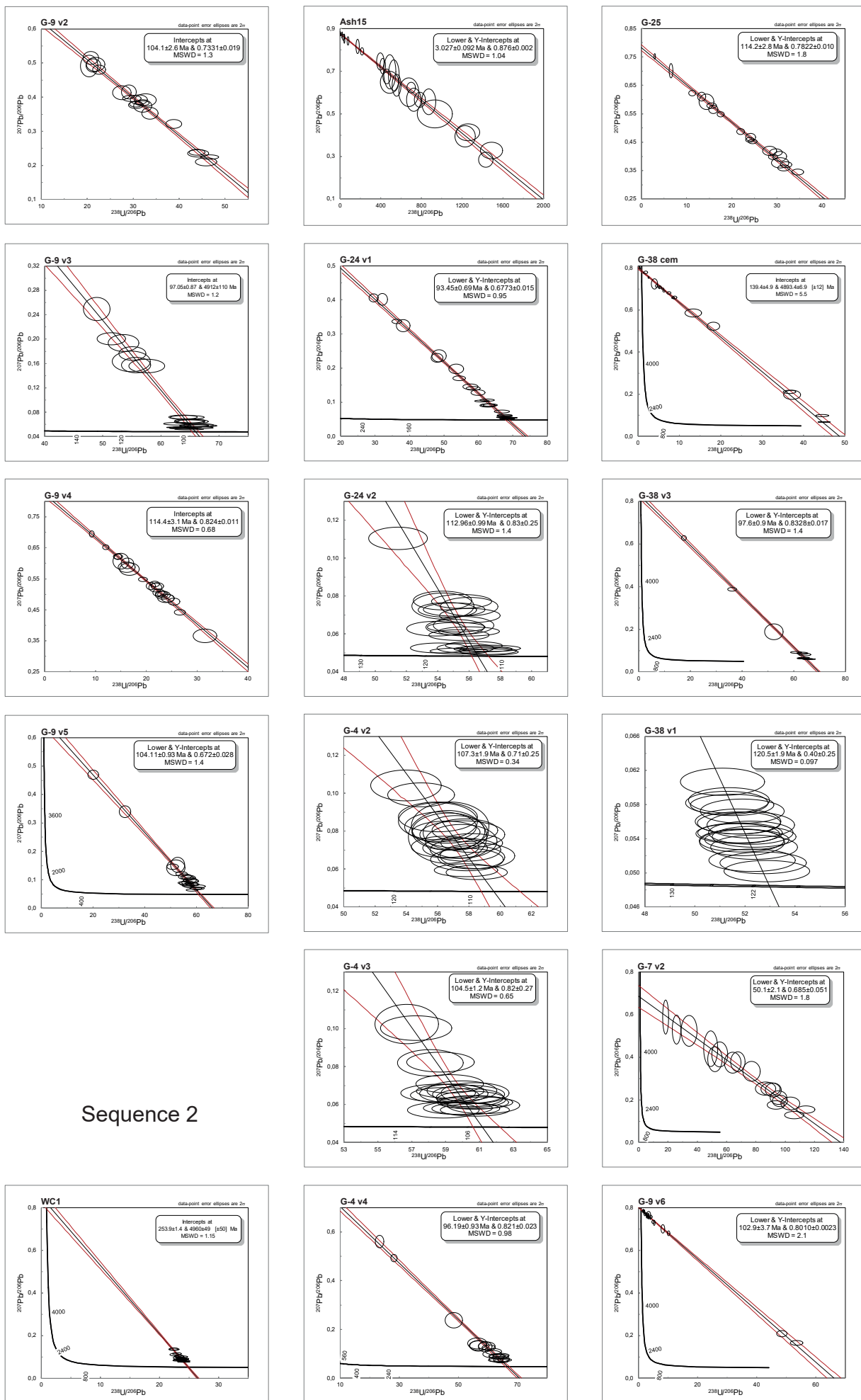


Figure S1: Tera-Wasserburg diagrams for each calcite phase measured in the U-Pb analysis.



Sequence 2

Figure S1: (continued).

S2: Minor element concentration diagrams of all analyzed calcite cement and vein phases.

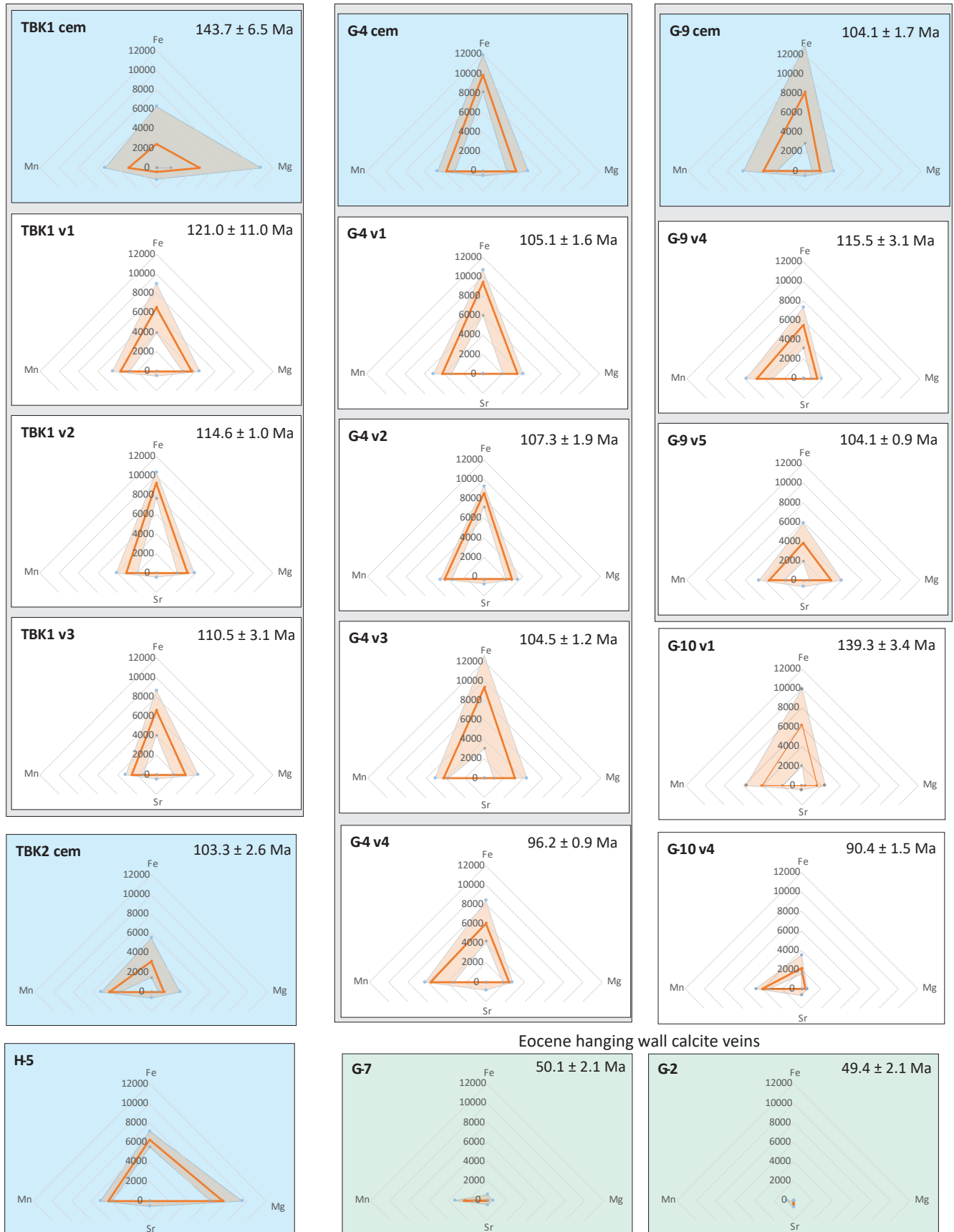


Figure S2: Diagrams showing the element concentrations of Fe, Mn, Mg, Sr of all measured calcite cement and vein generations. Diagrams with blue background refer to cements, with white background to veins, with green background to Eocene veins, and grey to basement and fault core veins. The black frame groups cement and vein generations of one sample. Where available for the respective cement and vein generation, U-Pb calcite ages are provided in upper right corner of each diagram.

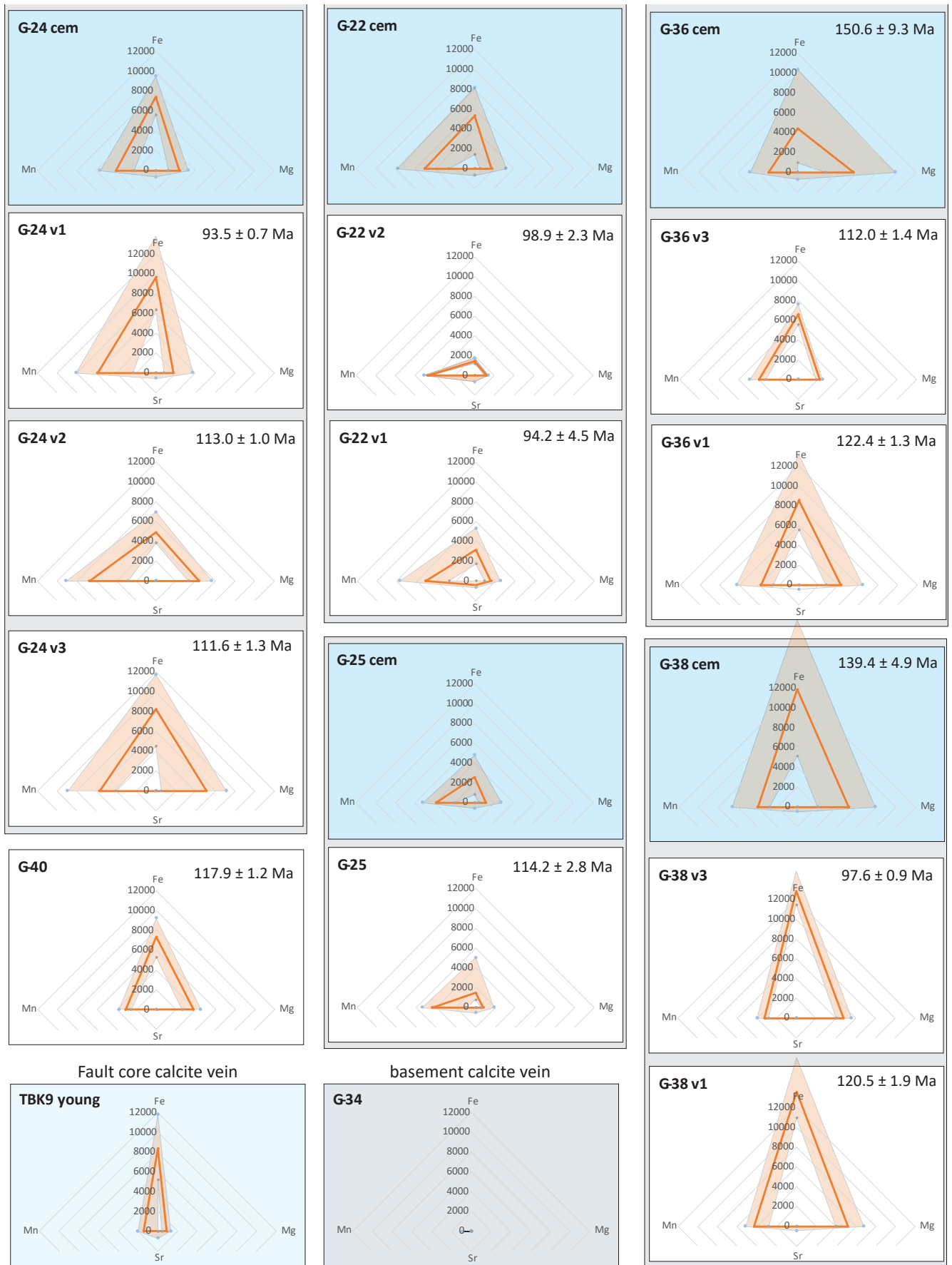


Figure S2: (continued).

S3: Sample Localities

Table S1: Sample Localities.

Sample	Latitude	Longitude	type	Lithology / stratigraphic formation
G-2	74.542062°	-20.671969°	calcite vein	Lindemans Bugt Formation
G-4	74.617573°	-20.801874°	calcite vein with cemented sandstone wall rock	Lindemans Bugt Formation
G-7	74.616583°	-20.792948°	calcite vein	Lindemans Bugt Formation
G-9	74.614542°	-20.792949°	calcite vein with cemented sandstone wall rock	Lindemans Bugt Formation
G-10	74.614542°	-20.792949°	calcite vein	Lindemans Bugt Formation
G-22	74.617714°	-20.805125°	calcite vein with cemented sandstone wall rock	Lindemans Bugt Formation
G-24	74.617714°	-20.805125°	calcite vein with cemented sandstone wall rock	Lindemans Bugt Formation
G-25	74.614824°	-20.807134°	calcite vein with cemented sandstone wall rock	Lindemans Bugt Formation
G-27	74.612632°	-20.800874°	cemented sandstone	Lindemans Bugt Formation
G-34	74.638782°	-20.830577°	calcite vein with gneiss wall rock	basement
G-36	74.626854°	-20.793191°	calcite vein with cemented sandstone wall rock	Lindemans Bugt Formation
G-38	74.626854°	-20.793191°	calcite vein with cemented sandstone wall rock	Lindemans Bugt Formation
G-40	74.625263°	-20.801344°	calcite vein with cemented sandstone wall rock	Lindemans Bugt Formation
G-41	74.625263°	-20.801344°	cemented sandstone	Lindemans Bugt Formation
G-42	74.625263°	-20.801344°	cemented sandstone	Lindemans Bugt Formation
G-43	74.625295°	-20.805417°	cemented sandstone	Lindemans Bugt Formation
G-44	74.625295°	-20.805417°	uncemented sandstone	Lindemans Bugt Formation
G-47	74.624326°	-20.803572°	uncemented sandstone	Lindemans Bugt Formation
G-48	74.630671°	-20.656902°	uncemented sandstone	Lindemans Bugt Formation
G-49	74.625113°	-20.652759°	uncemented sandstone	Lindemans Bugt Formation
G-57	74.628168°	-20.711449°	uncemented sandstone	Lindemans Bugt Formation
G-58	74.628168°	-20.711449°	uncemented sandstone	Lindemans Bugt Formation
G-60	74.628168°	-20.711449°	uncemented sandstone	Lindemans Bugt Formation
H-1	74.624861°	-20.626389°	uncemented sandstone	Lindemans Bugt Formation
H-2	74.624861°	-20.626389°	uncemented sandstone	Lindemans Bugt Formation
H-5	74.625583°	-20.634861°	cemented sandstone	Lindemans Bugt Formation
H-6	74.625583°	-20.634861°	cemented sandstone	Lindemans Bugt Formation
H-7	74.625583°	-20.634861°	cemented sandstone	Lindemans Bugt Formation
H-12	74.624028°	-20.804306°	cemented sandstone	Lindemans Bugt Formation
H-13	74.624028°	-20.804306°	cemented sandstone	Lindemans Bugt Formation
H-14	74.624028°	-20.804306°	cemented sandstone	Lindemans Bugt Formation
TBK1	74.615847°	-20.808716°	vein with cemented sandstone wall rock	Lindemans Bugt Formation
TBK2	74.615847°	-20.808716°	cemented sandstone	Lindemans Bugt Formation
TBK9	74.614632°	-20.820748°	calcite and dolomite vein with brecciated basement rock	Dombjerg Fault